Characterizing the Structure of pH Dependent Polyelectrolyte Block Copolymer Micelles

Albert S. Lee and Alice P. Gast*

Department of Chemical Engineering, Stanford University, Stanford, California 94305-5025

Vural Bütün and Steven P. Armes

School of Chemistry, Physics and Environmental Science University of Sussex, Brighton BN1 9QJ, E. Sussex, UK

Received December 1, 1998; Revised Manuscript Received April 20, 1999

ABSTRACT: We use fluorescence spectroscopy, dynamic light scattering (DLS), and small-angle neutron scattering (SANS) to characterize the structure of 2-(dimethylamino)ethyl methacrylate/2-(diethylamino)-ethyl methacrylate (DMAEMA/DEAEMA) block copolymer micelles. The copolymers exhibit a strong pH dependence, where protonation of the tertiary amines along the side chains cause the blocks to be soluble in water. Fluorescence results show a critical degree of protonation below which single chains aggregate to form micelles. This critical degree of protonation depends on the copolymer concentration and solution ionic strength. Dynamic light scattering experiments provide unimer and micelle size distributions, and the measured critical degrees of protonation are consistent with the fluorescence data. The micelle hydrodynamic radius measured from DLS depends on the solution ionic strength, because of the polyelectrolyte nature of the protonated copolymers. Small-angle neutron scattering experiments in conjunction with a starlike micelle model provide additional insights into the micellar structures.

Introduction

The study of micellar systems constitutes a broad area of research and applications ranging from household soaps to drug delivery systems. One specific class of micelles, polymeric micelles, comprise a copolymer having soluble and insoluble blocks, where the insoluble blocks aggregate to form a dense core and the soluble blocks extend out into the solvent to form a corona.[1,2] These micelles can assume various shapes, ranging from wormlike to spherical micelles.[3,4] In the past decade, the area of research in block copolymer micelles has been growing, and recently more attention has been focused in the area of aqueous block copolymer micelle systems. In general, aqueous copolymer systems have been difficult to prepare and to work with, often requiring a cosolvent such as methanol or THF to adequately dissolve the polymers to form stable, well-behaved micelles.[5]

One way to avoid the use of cosolvents is to use block copolymers which are sensitive to the solution pH, where below a certain critical pH the copolymers dissolve as unimers and aggregate to form micelles as the pH is increased beyond a critical value.[6−8] Recently Armes et al. have synthesized 2-(dimethylamino)-ethyl methacrylate/2-(diethylamino)ethyl methacrylate (DMAEMA/DEAEMA) copolymers which form micelles in aqueous solution above a critical pH.[6] The structures are shown in Figure 1. Under acidic conditions, the amine groups on the side chains are protonated, causing the copolymers to become hydrophilic and to remain as unimers in solution. Protonation of the side chains also causes the copolymers to behave as polyelectrolytes. The subsequent addition of base deprotonates the side chains, causing the DEAEMA block to become hydrophobic. Above a critical pH, the copolymers aggregate to form micelles. The DEAEMA block forms the micelle core while the hydrophilic DMAEMA block extends out into the solvent to form the micelle corona. When excess base is added, the whole copolymer becomes deprotonated, causing the micelles to aggregate and come out of solution. These copolymers could serve as a model for a delivery system, where the solute encapsulated in the micelle cores is released as the micelles break apart when they reach a target pH.[8]

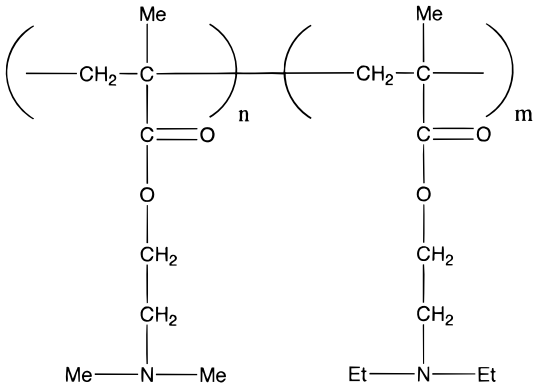

Figure 1. DMAEMA/DEAEMA block copolymer structure.

In this study, we use light scattering, fluorescence spectroscopy, and neutron scattering techniques to characterize the structure of DMAEMA/DEAEMA block copolymer micelles. We seek to find critical parameters such as the critical degree of protonation along the chain when micellization occurs. Because of the pH dependence and the weak polyelectrolyte nature of the copolymers, we expect a rich structural dependence of the unimers and micelles on parameters such as the solution ionic strength and pH.

Experimental Section

Materials. The DMAEMA/DEAEMA block copolymers were synthesized at Sussex using group transfer polymerization. The details of the synthesis are reported elsewhere.[6] Gel permeation chromatography analysis

10.1021/ma981865o CCC: $18.00
Published on Web 06/04/1999

indicated a copolymer molecular weight of 32 600 with M_w/M_n of 1.10. Proton NMR spectroscopy confirmed the DMAEMA content to be 51 mol %. By using helium pycnometry, the solid state density of DEAEMA homopolymer was measured to be 1.046 g/mL.

Samples were prepared by dissolving the copolymer in Milli-Q deionized water titrated to pH 2 with HCl. Upon addition of the DMAEMA/DEAEMA copolymer, the pH increases to between 2 and 3, because of the basic nature of the amine groups along the polymer side chains. Additional HCl was added to return the solution pH to 2, to ensure complete dissolution of the copolymer. These samples are slowly titrated using KOH to higher pHs to form micelles. Samples were gently agitated overnight with a magnetic stirbar before experiments were performed.

For the titrations, acid and base solutions of HCl and KOH were each prepared at 1 M and 0.1 M concentrations. Titrations with 0.5030 M HCl (Aldrich) or 0.4936 M NaOH (Aldrich) standards were used to standardize the prepared acid and base solutions.

Pyrene was used as a fluorescent probe to detect the presence of micelles by fluorescence. Pyrene (Aldrich) was dissolved in acetone (Baker) at a known concentration and added to empty vials. After evaporation of the acetone, the polymer samples were added to the vials. The added volume of pyrene solution was calculated such that the final pyrene concentration in the sample would become approximately 6×10^{-7} M, which is near the saturation concentration of pyrene in water. Before addition of pyrene, the copolymer solutions were allowed to equilibrate overnight with stirring. Upon addition of pyrene, these solutions were stirred one more night before measurements were taken.

Potentiometric Titrations. A Rainin motorized pipette (EDP Plus) with a 100 μL liquid end was used to deliver known amounts of standardized HCl or KOH to the samples. An Orion 611 pH meter with a semimicrocombination electrode (Orion Ross 8103) was used to monitor the pH during the titrations. Because of the tendency of the measured sample to drift over long periods of time, the accuracy of the pH is estimated to be approximately 0.05 pH units. Titration curves were generated by first titrating the solution to pH 2 with 1 M HCl to ensure complete dissolution of the copolymer and then slowly adding 0.85 or 0.085 M KOH in 10 to 100 μL increments while measuring the pH after each increment.

As HCl and KOH are added during the titrations, K^+ and Cl^- ions are unavoidably added. The effective amount of KCl added is approximately 0.018 M after the titrations to form the micelles. A "low salt" sample was also prepared, where, instead of initially titrating with HCl to pH 2, the samples are titrated to pH 3.5 before titrating with KOH to form the micelles. The effective concentration of KCl added for the low salt micelles amounts to approximately 0.006 M.

Fluorescence Spectroscopy. Steady-state fluorescence measurements were taken with an SLM-Amino 8100 fluorescence spectrometer. All spectra were taken at room temperature with an integration time of 0.1 s and a bandpass of 4 nm. The emission spectra were taken with the excitation wavelength λ_{ex} at 333 nm, corresponding to the strongest excitation peak for pyrene in water, and the excitation spectra were taken with the emission wavelength λ_{em} at 394 nm, the strongest emission peak. We average the results from three repetitions of each emission and excitation measurement. The spectra are consistent between repetitions, with a standard deviation below 2%.

Dynamic Light Scattering. The dynamic light scattering (DLS) measurements were performed with a 2 W Lexel model 95 argon ion laser at a wavelength of 514.5 nm and at a power of 150−300 mW. A Brookhaven Instruments BI-200 goniometer was used to measure the scattered light intensity at scattering angles of 33.07, 56.93, 90.00, 123.07, and 146.93°, corresponding to the scattering vector q ranging from 0.0093 to 0.0312 nm^{-1}. Samples were filtered through 0.2 μm syringe filters (Whatman Anotop) into glass fluorescence cells (Spectrocell). Prior to sample loading, the cells were soaked overnight in 70/30 v/v sulfuric acid/hydrogen peroxide solution and thoroughly cleaned with filtered Milli-Q water. Special caution was taken when handling the acid cleaner. Data were collected over a duration ranging from 4 to 30 min, depending on the amount of scattering from the sample, and the data was stored and processed on a Brookhaven Instruments BI-9000 correlator. Measurements were taken at 25 °C, as maintained by a Neslab circulating bath.

For a system with a distribution of sizes, the autocorrelation function $g^{(1)}(\mathbf{q}, \tau)$ takes the form[9]

$$g^{(1)}(\mathbf{q}, \tau) = \int_0^\infty F(R_h)\exp\left[-\frac{q^2kT}{6\pi\mu}R_h^{-1}\tau\right] dR_h + \Delta \quad (1)$$

The characteristic decay times of the autocorrelation function depend on parameters such as the solution viscosity μ and the thermal energy kT. Scattering from large impurities such as dust contributes the autocorrelation function as an additive "dust term" Δ. The filtered samples were generally dust-free, and the dust term was usually well below 0.01. Sample runs with dust terms greater that 0.01 were disregarded.

The R_h distribution is weighted by the intensity $F(R_h)$. The autocorrelation data was analyzed using CONTIN,[10,11] a FORTRAN program which uses a constrained Laplace transform of the data to find an optimum $F(R_h)$ size distribution which, when used with eq 1, causes $g^{(1)}(\mathbf{q}, \tau)$ in eq 1 to best fit the data. The CONTIN program also integrates over each peak in the size distributions to find a weighted average $\bar{R}_h$ for each peak.

For each sample, we take three to five repeated measurements at a scattering angle of 90°. We report the average of the data at this scattering angle for the $F(R_h)$ size distributions and $\bar{R}_h$ values. Along with these measurements at 90°, one measurement was taken at each of the remaining scattering angles.

Small-Angle Neutron Scattering. Small-angle neutron scattering (SANS) measurements were performed at the National Institute of Standards and Technology (NIST) Center for Neutron Research (NCNR) in Gaithersburg, MD. Measurements were taken at the 8 m SANS on beamline NG7 with an incident wavelength λ = 9 Å and a sample-to-detector distance of 3.6 m. Sample cells of 1 mm path length were used. Data were collected on a two-dimensional detector giving scattering vectors q ranging from 5×10^{-4} to 0.12 $Å^{-1}$. The scattering profiles were corrected for background and empty cell scattering, and effects from solvent scattering were subtracted.

DMAEMA homopolymer and DMAEMA/DEAEMA copolymer micelle solutions were prepared as described above, using D_2O (Isotec) as the solvent and titrating with DCl and KOD (Aldrich) to a final pH of 7.7. The homopolymer sample was titrated in the same way as the micelles to match the homopolymer solution conditions with those of the micelles. Higher polymer concentrations were used to improve the measured scattered signal, with the homopolymer and copolymer at concentrations of 0.01 and 0.005 g/mL, respectively. Complementary DLS experiments were performed on these same deuterated samples to measure micelle and homopolymer hydrodynamic radii.

Starlike Micelle Model. We compare our experimental results with a model for starlike micelles. In this section, we briefly present an outline of the starlike micelle model developed by Vagberg et al.,[12] on the basis of the work of Daoud and Cotton.[13] The model describes the micelle as a spherical core surrounded by a shell of chains extending out into the solvent, as in a star. The model describes the coronal shell as a series of connected blobs whose sizes increase with increasing distance away from the core. Each blob is defined as a part of a coronal chain which undergoes a self-avoiding random walk. We use the model to predict the micelle core radius R_c, micelle radius R_m, and radius of gyration R_g.

The micelle density profile $\rho(r)$ as a function of distance r from the micelle center can be described as

$$\rho(r) = \rho_c \quad r < R_c$$
$$\rho(r) = A(r/a_s)^{1/\nu} r^{-3} \quad R_c < r < R_m$$
$$\rho(r) = 0 \quad R_m < r \tag{2}$$

where A is a constant of proportionality [$A = 3(4^{1/\nu}) f^{(3\nu-1)/2\nu}/32\pi$], ρ_c is the core segment density, a_s is the statistical segment length in the micelle corona, and the Flory exponent ν takes values of $^1/_2$ and $^3/_5$ in θ and good solvent conditions, respectively. Integration of the density profile over the micelle volume and matching with the known total number of monomers within this volume gives expressions for the core radius

$$R_c = \left(\frac{3N_c f}{4\pi\rho_c}\right)^{1/3} \tag{3}$$

and the micelle radius

$$R_m = \left(\frac{8N_s f^{(1-\nu)2\nu}}{3 \times 4^{1/\nu}\nu} a_s^{1/\nu} + R_c^{1/\nu}\right)^{\nu} \tag{4}$$

where N_c and N_s are the number per block copolymer chain of core and shell segments, respectively, and f is the number of arms in the star.

The radius of gyration R_g as measured by SANS is the second moment of the scattering length density $\rho^N(r)$[12,14]

$$\langle R_g^2 \rangle = \frac{\int_0^\infty \rho^N(r) r^4 \, dr}{\int_0^\infty \rho^N(r) r^2 \, dr} \tag{5}$$

where $\rho^N(r)$ varies along the micelle profile as

$$\rho^N(r) = (\rho^N{}_c - \rho^N{}_o) \quad r < R_c$$
$$\rho^N(r) = (\rho_s^N - \rho_o^N) A V_s (r/a_s)^{1/\nu} r^{-3} \quad R_c < r < R_m$$
$$\rho^N(r) = 0 \quad R_m < r \tag{6}$$

and ρ_c^N, ρ_s^N, and ρ_o^N are scattering length densities of the core segments, shell segments, and the solvent, respectively. The term V_s represents the volume of a statistical segment in the shell. Integration of eq 5 results in

$$\langle R_g^2 \rangle = \frac{\left(\frac{\rho_c^N - \rho_o^N}{5}\right) R_c^5 + \frac{(\rho_s^N - \rho_o^N) A V_s}{a_s^{1/\nu}} \left(\frac{1}{1/\nu+2}\right) (R_m^{1/\nu+2} - R_c^{1/\nu+2})}{\left(\frac{\rho_c^N - \rho_o^N}{3}\right) R_c^3 + \frac{(\rho_s^N - \rho_o^N) A V_s}{a_s^{1/\nu}} \nu (R_m^{1/\nu} - R_c^{1/\nu})} \tag{7}$$

Estimates of the scattering length densities ρ_c^N, ρ_s^N, and ρ_o^N were calculated by summing over the scattering lengths of the atoms in each molecule[15] and are tabulated in Table 1. We estimate the scattering length density of the DMAEMA/DEAEMA copolymer ρ_{bcp}^N as the average of ρ_c^N and ρ_s^N.

Results and Discussion

Potentiometric Titration Curves. As described earlier, we measure titration curves by first using HCl to titrate the polymer solutions to pH 2 and then monitoring the pH as we gradually add KOH. Figure 2a shows a titration curve for the copolymer at 0.001 g/mL, where the bottom axis represents the net amount of HCl added and the titration occurs sequentially from right to left. The copolymer behaves as a weak base and buffers the solution at a pH around 7, as shown in the plateau region of the titration curve. At a pH of around 9, at the second inflection point, the solution becomes turbid as the micelles aggregate and come out of solution. As a reference, a calculated titration curve for pure water is also included in Figure 2a, accentuating the buffering effect of the copolymers.

We also obtain titration curves for each individual homopolymer at a concentration which matches the corresponding block concentration in the 0.001 g/mL copolymer sample. The titration curves are also shown in Figure 2a, and from these titrations, we obtain pK_a values of 6.9 and 6.6 for the conjugate acid DEAEMA$^+$ and DMAEMA$^+$ homopolymers, respectively. Considering the dependence of the pK_a on the solution conditions, the measured pK_a of 6.6 for DMAEMA generally agrees with those reported for DMAEMA in the literature.[16,17] The stronger basicity of DEAEMA is expected, as amines with ethyl groups are known to be more basic than amines with methyl groups.[18] Analogous amines such as trimethylamine have much higher pK_a's ranging between 9 and 10. The unusually low pK_a of DMAEMA relative to small molecules has been reported to be caused by a cyclization of the side chain conformation such that the amine group is stabilized by the carbonyl group in the side chains.[16]

The titrations of the homopolymers provide insight into the behavior of the block copolymer. At 22 °C, the DMAEMA homopolymer remains in solution at all pHs,

Table 1. SANS Scattering Length Densities ρ^N

molecule	$\rho^N \times 10^{-9}$ (cm^2)
DMAEMA (ρ_s^N, ρ_h^N)	8.3
DEAEMA (ρ_c^N)	6.4
DMAEMA/DEAEMA (ρ_{bcp}^N)	7.3
D_2O (ρ_o^N)	63.7

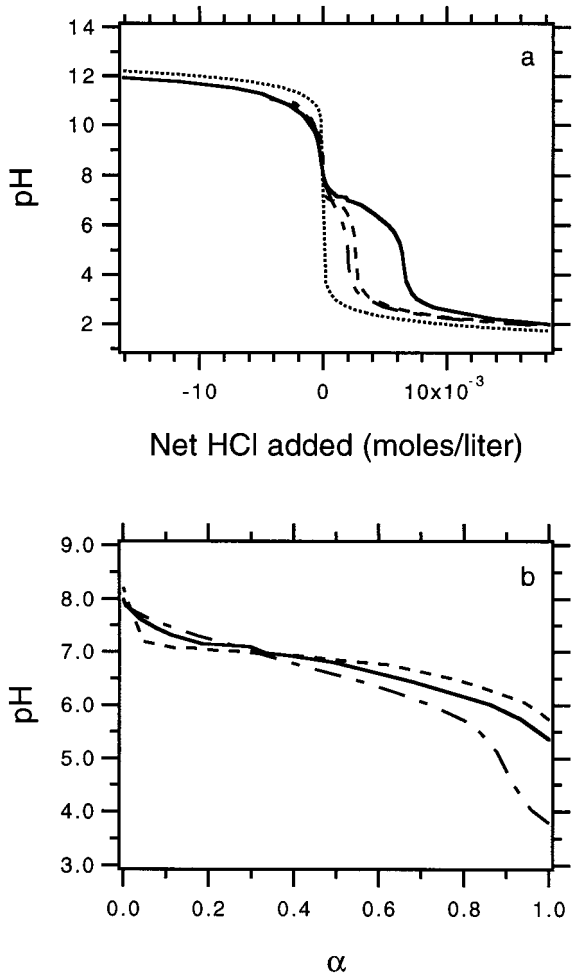

Figure 2. (a) Titration curves of (—) 0.001 g/mL DMAEMA/DEAEMA copolymer, (- - -) 0.0005 g/mL DEAEMA homopolymer, (— - —) 0.0005 g/mL DMAEMA homopolymer, and (···) pure water. (b) Same titration curves as in part a with the *x* axis expressed as the degree of protonation α.

indicating that DMAEMA remains hydrophilic even when fully deprotonated. The DEAEMA homopolymer precipitates out of solution at pH greater than 8, confirming that deprotonation of the DEAEMA block in the copolymer induces micelle formation. The relative pK_a values of the homopolymers reveal that during titration of the copolymer the less basic amine groups in the DMAEMA blocks deprotonate more easily than those in the DEAEMA blocks, such that, by the time enough base is added to deprotonate the DEAEMA blocks to induce the micellization, many of the amine groups in the DMAEMA blocks in the corona are deprotonated and uncharged.

Titrations of 0.001 g/mL copolymer samples with low salt, no added KCl, and 0.04 M added KCl are plotted in Figure 3a. The effective amount of KCl added for each of these solutions is 0.006, 0.018, and 0.022 M, respectively. Increases in the salt concentration shifts the plateau to a slightly higher pH. Pradny and Seveik have demonstrated that DMAEMA homopolymer becomes

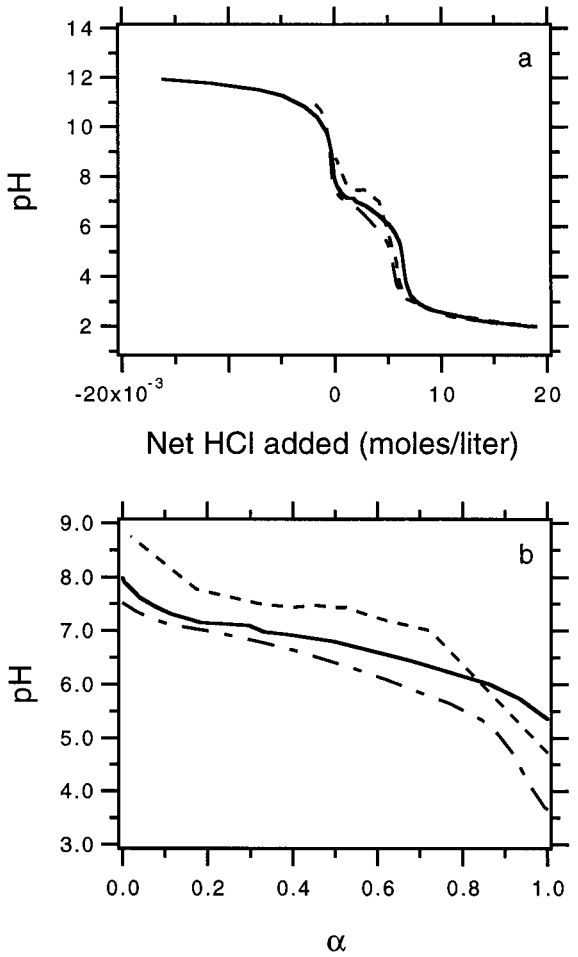

Figure 3. (a) Titration curves of 0.001 g/mL DMAEMA/DEAEMA with varying salt concentrations of (— - —) low salt, (—) no added KCL, and (- - -) 0.04 M KCl. The effective amounts of KCl added for these are 0.006, 0.018, and 0.022 M, respectively. (b) Same titration curve as in part a with the *x* axis expressed as α.

more acidic as the degree of side chain protonation increases because of mutual repulsion of the protons along the chain.[16] Increasing KCl concentrations causes screening of the charges along the polymer, decreasing the acidity and increasing the effective pK_a of the copolymer.

We define α as the ratio C_H/C_m, where C_H is the effective concentration of added HCl and C_m is the concentration of polymer chains in terms of monomeric units. When defined in this way, α approximates the degree of protonation, or the fraction of amine groups in the copolymer chain which are protonated, assuming that all of the H^+ from the added HCl protonate the amine groups. The titration curves plotted as a function of α for $0 < \alpha < 1$ are shown in the Figures 2b and 3b. We define α* as the critical α, where the transition from unimers to micelles takes place as α decreases below α*. Similarly, we define the corresponding critical pH as pH*, where micelles form at pHs greater than pH*. Describing the net amount of acid added in terms of α and pH gives two pictures of what is happening in the sample. The term α describes the degree of protonation of the polymer, whereas the pH describes the solvent environment surrounding the polymer. In the plateau region of the titration curves, α can change significantly while the pH remains fairly constant. In this buffering region, the pH does not seem to fully depict what is

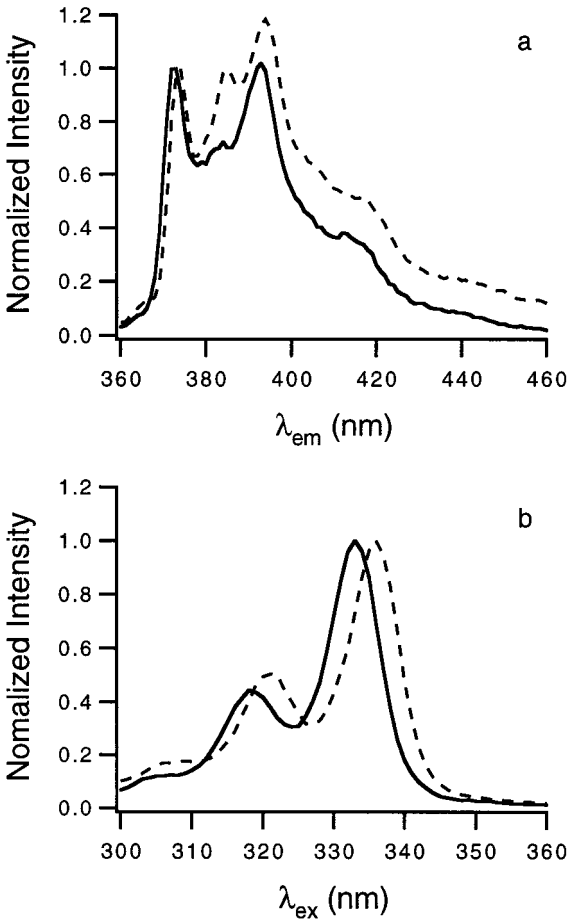

Figure 4. (a) Emission spectra of pyrene in the presence of (—) unimers and (- - -) micelles. (b) Excitation spectra of pyrene in the presence of (—) unimers and (- - -) micelles.

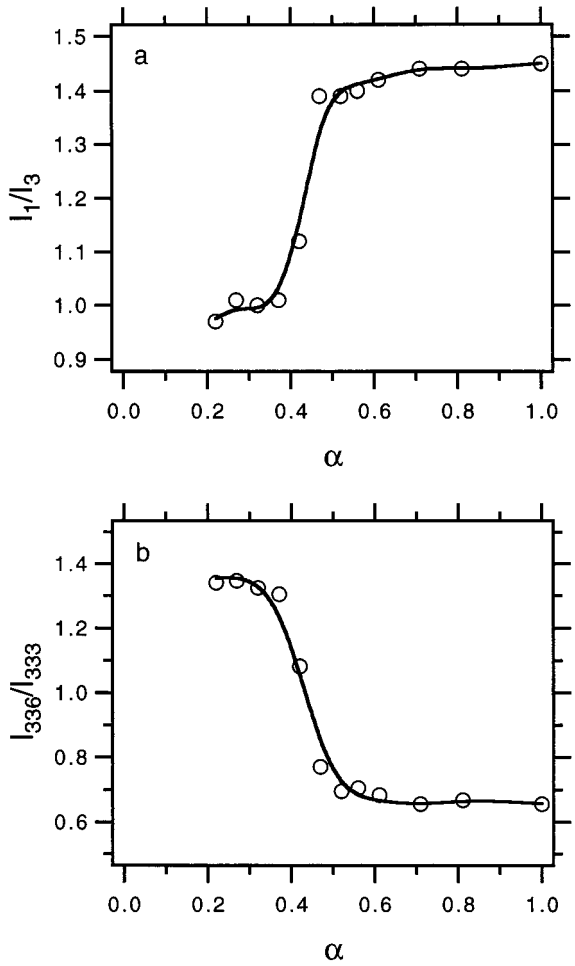

Figure 5. (a) I_1/I_3 intensity ratios from emission spectra of 0.001 g/mL DMAEMA/DEAEMA as a function of α. (b) I_{336}/I_{333} intensity ratios from excitation spectra of 0.001 g/mL DMAEMA/DEAEMA as a function of α. For parts a and b, lines have been placed to guide the eye.

happening to the polymer as acid or base is added. However, upon closer examination of Figures 2b and 3b, we see that changes in the pH weakly correlate with changes in α even in the plateau region of the titration curve. In this way, both α and pH are useful in describing the effect of adding acid or base, although α is more useful to paint a more detailed picture of the physics involved during micellization.

Fluorescence Experiments. We use fluorescence spectroscopy to determine the presence of micelles in our copolymer solutions. We use pyrene as a probe which preferentially partitions into the hydrophobic micelle cores. As shown in Figure 4, the emission and excitation spectra of pyrene vary depending on the surrounding environment.[19,20] In the emission spectra in Figure 4a, the third intensity peak is higher when pyrene is in the hydrophobic micelle core rather than in water. As shown in the excitation spectra in Figure 4b, the intensity peak at 333 nm shifts to higher wavelengths when pyrene is surrounded by a hydrophobic environment. The differences in the emission spectra can be characterized by the intensity ratio of the first and third peaks, I_1/I_3, where a low I_1/I_3 indicates the presence of micelles.[19,20] Similarly, the excitation spectra can be characterized by the I_{336}/I_{333} ratio, where a high I_{336}/I_{333} ratio reflects the presence of micelles.[20] Figure 5 shows the I_1/I_3 and I_{336}/I_{333} ratios plotted as a function of α. The transition from unimers to micelles can be identified by the inflections of the I_1/I_3 and I_{336}/I_{333} plots. For the 0.001 g/mL sample, both plots indicate an α* of 0.45, with a pH* of 7.2. The fluorescence measurements show that as base is added and α decreases during micellization, micelles do not form until just over half of each copolymer is deprotonated. The slightly higher acidity of the protonated amine groups in the DMAEMA chain leads us to believe that more of the DMAEMA blocks are deprotonated than the DEAEMA blocks when α* is reached. Once the micelles are formed, much of the DMAEMA blocks which form the coronae are deprotonated, and we do not expect the coronal chains to behave as strong polyelectrolytes.

We also obtained I_1/I_3 plots for 0.001 g/mL samples with varying salt concentration by adding KCl, but the salt caused pyrene to come out of solution, leading to ambiguous I_1/I_3 plots. The results show the general trend that increasing salt concentration causes α* to shift to higher values and pH* to lower values. The salt screens repulsive interactions between the charged chains, allowing the chains to aggregate more easily at higher acid concentrations.

Dynamic Light Scattering Measurements. We use DLS to obtain micelle size distributions. Measurements of micelles at varying copolymer concentrations yield a consistent hydrodynamic radius, $\bar{R}_h$, of 26 nm, suggesting closed association. We vary the acid concentration to find α* and pH*. Figure 6 shows the size distributions at four different pHs. At $\alpha \geq 0.53$ or pH ≤ 7.2, the polymer chains remain as unimers, and the size distribution shows a narrow peak at a hydrodynamic

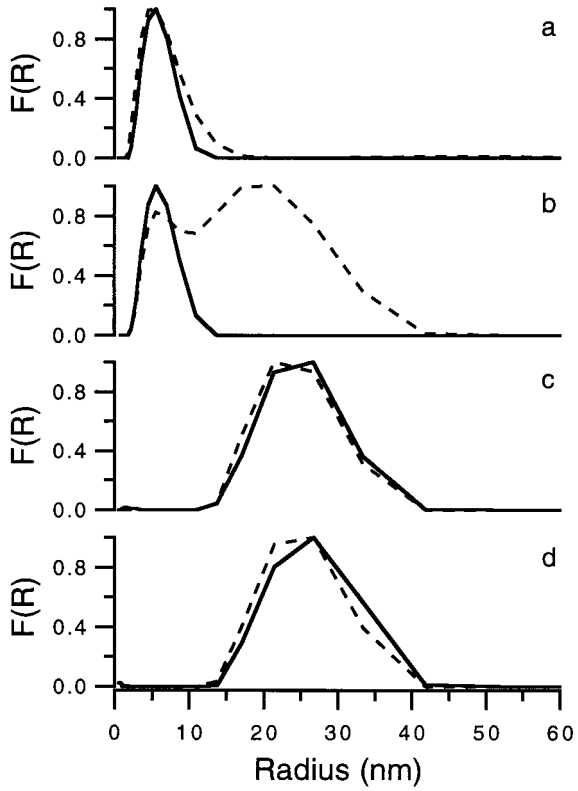

Figure 6. DLS CONTIN micelle and unimer size distributions for (—) no added KCl and (- - -) 0.02 M added KCl at (a) $\alpha = 0.61$ and pH = 7.0, (b) $\alpha = 0.53$ and pH = 7.2, (c) $\alpha = 0.31$ and pH = 7.4, and (d) $\alpha = 0.23$ and pH=7.6.

radius of 6 nm. At $\alpha \leq 0.31$ or pH ≥ 7.4, the unimer peak disappears, and a new broader peak appears at a hydrodynamic radius of 26 nm. These results agree with the α^* of 0.45 and pH* of 7.2 obtained from the fluorescence measurements.

We notice in Figure 6 that once the micelles are formed, the micelle size does not depend on α or pH. If the DMAEMA blocks were heavily protonated, we would expect the micelle corona to swell because of repulsive forces when α increases as the pH is increased. Theoretical scaling arguments show that if the micelle corona is charged, the micelle radius should increase as $p^{4/7}$, where p is the fractional charge on the coronal chains;[21] however, the micelle sizes for $\alpha = 0.31$ and 0.23 are essentially the same. This lack of dependence of R_h on α confirms that during micellization most of the DMAEMA block is already deprotonated and that the chains in micelle corona are only weakly charged.

Also shown in Figure 6 are size distributions from the same copolymer solutions with 0.02 M KCl added. Upon addition of salt, the unimer chains with $\alpha = 0.53$ and pH = 7.2 begin to aggregate to form micelles, as can be seen by the appearance of a second peak corresponding to micelles. As we observed from the fluorescence measurements, the DLS measurements also show that adding salt raises α^* and lowers pH*.

In addition to the effect of salt on α^* and pH*, we use DLS to investigate the effect of salt on the average micelle hydrodynamic radius $\bar{R}_h$. Figure 7 shows $\bar{R}_h$ as a function of salt concentration for a 0.001 g/mL copolymer solution with $\alpha = 0.19$ and pH= 7.8. For these measurements, salt was incrementally added to a micelle solution with DLS measurements made after each addition. The DLS measurements indicate that the micelle $\bar{R}_h$ does not depend on salt concentration. The

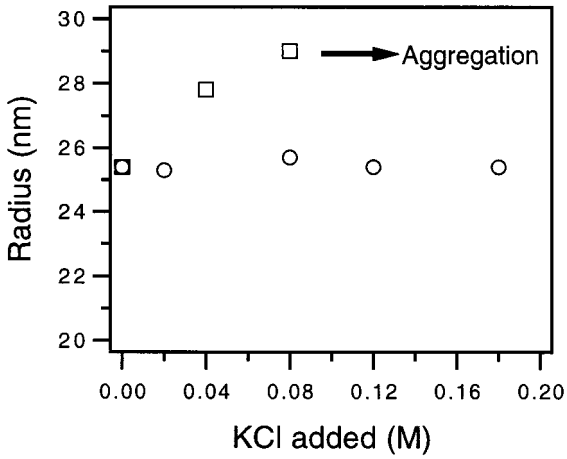

Figure 7. $\bar{R}_h$ versus added KCl, with (○) KCl added at pH = 7.8 after titration to form micelles and (□) KCl added at pH = 2.0 prior to titration to form micelles.

salt was expected to affect $\bar{R}_h$ in two possible ways. If the coronal blocks were charged, the salt would screen the electrostatic repulsions in the micelle corona, causing the chains in the corona to be less stretched with a smaller micelle $\bar{R}_h$. The second effect we anticipated upon addition of salt is the screening of the repulsive interchain interactions to allow more chains to aggregate to form larger micelles with higher aggregation numbers. However, we do not see coronal contraction or larger aggregation numbers, as R_h in Figure 7 remains constant. It is possible that the two effects offset each other. A more probable picture is that after the micelles are formed and brought to pH 7.8, most of both of the DMAEMA and DEAEMA blocks are deprotonated such that the micelle looks like a nonionic micelle. In this case, we would not expect any salt dependence.

We gain additional insight by performing DLS experiments on micellar solutions prepared slightly differently than above. Instead of adding salt after micellization, salt was added before starting the titrations to form micelles. Figure 7 includes $\bar{R}_h$ versus salt concentration plots with the second preparation method. The solutions prepared by adding salt prior to micellization show larger micelles for larger initial salt concentrations. At a salt concentration near 0.1 M, the micelles begin to aggregate. This dependence of $\bar{R}_h$ on the initial salt concentration indicates a competition between hydrophobic attractions and electrostatic repulsions near α^*. As the DEAEMA block is deprotonated during titration, it reaches an α where the DEAEMA becomes more hydrophobic than hydrophilic and tends to aggregate; however, at this α, the chains are not fully deprotonated and electrostatic repulsions between the chains hinder micellization. The salt which was present before the start of the titration screens the charges on the amine groups, reducing electrostatic repulsions and allowing more chains to aggregate to form micelles with larger $\bar{R}_h$. Once the micelles are formed and the pH brought up to 7.8, the chains that form the micelle are almost fully deprotonated, and further addition of salt does not increase $\bar{R}_h$. This hysteretic behavior corresponds to the differences in the titrations curves shown in Figure 3. The presence of salt in the solution alters the copolymer association behavior as well as its buffering capacity. Small-angle X-ray scattering (SAXS) and SANS experiments planned for the future will further elucidate this salt-dependent micelle behavior.

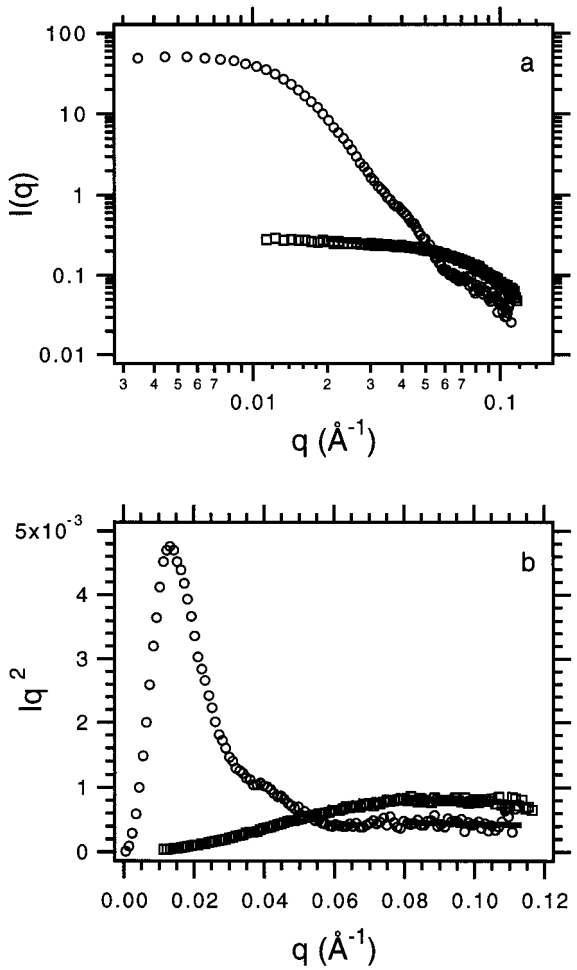

Figure 8. (a) SANS scattering profiles for (○) DMAEMA/DEAEMA micelles and (□) DMAEMA homopolymer. Homopolymer data is fitted to the Debye equation in eq 8. (b) Kratky plots of the same data as in part a for (○) DMAEMA/DEAEMA micelles and (□) DMAEMA homopolymer. Data are fit to $q^{1/\nu}$ scaling to obtain best fits for ν.

Small-Angle Neutron Scattering Results. Scattering profiles obtained from SANS at pH 7.7 are plotted in Figure 8a. At low q, the scattering profile of DMAEMA homopolymer varies greatly from that of the DMAEMA/DEAEMA copolymer micelles because of their large difference in size. The profiles at higher q values provide structural information at smaller length scales within the micelles and single chains. We fit the homopolymer scattering profile with the Debye equation[22] which predicts the scattering from isolated random coils

$$I(q) = I(0)\frac{2}{x^2}(x - 1 + e^{-x}) \tag{8}$$

Here x represents $(qR_g)^{1/\nu}$, where ν takes values of $^1/_2$ and $^3/_5$ for the θ and good solvent cases, respectively. From the fits of eq 8 to the homopolymer, we obtain R_g and $I(0)$ for the DMAEMA homopolymer. In the high q regime, $I(q)$ in eq 8 approaches a $q^{1/\nu}$ scaling, and this is seen in the plateau region of the Kratky plots in Figure 8b. From the Kratky plot, we see that both this homopolymer and the copolymer micelles follow a q^2 scaling for large q, indicating θ solvent conditions. Fitting a log−log plot of the scattering profile according to the $q^{1/\nu}$ scaling gives ν equal to 0.44 and 0.46 for the micelles and homopolymer, respectively, indicating sub-θ solvent conditions. We note that we have fit a relatively narrow q range to obtain ν and that these fitted values for ν are somewhat preliminary. The possible sub-θ scaling for the DMAEMA chains in solution as well as in the corona may reflect the interesting molecular structure of these polyacrylate amines.[16] The association between amine and carbonyl groups may cause cyclization with one monomer[16] or intrachain interactions that would appear as an effective segmental attraction.

We are able to obtain R_g and $I(0)$ for both the micelles and homopolymer by fitting the scattering profiles to the Guinier approximation,

$$I(q) = I(0)e^{-q^2R_g^2/3} \tag{9}$$

and the Zimm approximation,

$$\frac{1}{I(q)} = \frac{1}{I(0)}\left[1 + \frac{q^2R_g^2}{3}\right] \tag{10}$$

The Zimm approximation tends to overestimate R_g, and the Guinier approximation tends to underestimate R_g.[23] We report R_g as an average of the results of the Zimm and Guinier analyses.

The Zimm approximation comes from the Zimm equation,

$$\frac{K^Nc}{\Delta R} = \frac{1}{M_w}\left[1 + \frac{q^2\langle R_g^2\rangle}{3}\right] + 2A_2c \tag{11}$$

where c is the copolymer concentration, A_2 is the second virial coefficient, and M_w is the homopolymer or micelle molecular weight. K^N is an optical constant, $K^N = (\rho_1^N - \rho_o^N)^2/\rho_1^2N_A$ with polymer scattering length density ρ_1^N, polymer density ρ_1, and Avogadro constant N_A. The excess Rayleigh ratio ΔR in eq 11 is the difference between Rayleigh ratios ($R_{solution} - R_{solvent}$) of the solvent and copolymer solution. The Rayleigh ratio is defined as

$$R(\theta,c) = I(q)r^2/I_oV \tag{12}$$

and depends on the scattered intensity $I(q)$, intensity of the incident beam I_o, the scattering volume V, and the distance r between the scattering volume and detector. Assuming low copolymer concentrations and low solvent scattering, we can take a ratio of the Zimm equation in eq 11 for the homopolymer and micelles to obtain

$$\frac{M_{w,m}}{M_{w,h}} = \left(\frac{c_h}{c_m}\right)\left(\frac{\rho_h^N - \rho_o^N}{\rho_{bcp}^N - \rho_o^N}\right)\left(\frac{I(0)_m}{I(0)_h}\right) \tag{13}$$

where the subscripts m and h correspond to micelles and homopolymer, respectively. Here $\rho_h^N = \rho_s^N$ and we estimate the block copolymer scattering length density ρ_{bcp}^N as the average of ρ_s^N and ρ_c^N. Knowing the homopolymer molecular weight and the relative concentrations, we use eq 13 to estimate the micelle molecular weight and obtain an approximate value for the micelle aggregation number f. In addition, we can obtain a_s from the measured homopolymer R_g by assuming a Gaussian chain profile, where $R_g^2 = N_sa_s^2/6$, with N_s representing the number of statistical segments in the polymer coil.

Table 2. Parameters Used in the Starlike Micelle Model[a]

a_s (nm)	ρ_c (nm^{-3})	ν	f	N_c	N_s
1.7	0.73	0.44	173	17	18

[a] a_s, ν, f, N_c, and N_s are from SANS measurements.

Table 3. Results from Starlike Model and Experiments

characteristic	DMAEMA/DEAEMA micelle	DMAEMA homopolymer
Dynamic Light Scattering		
R_h (in D_2O, nm)	28.2	2.2
Small-Angle Neutron Scattering		
R_g		
Debye (nm)		2.1
Zimm (nm)	15.5	2.8
Guinier (nm)	12.6	2.7
average (nm)	14.1	2.6
molecular weight	5.64×10^6	12 300
aggregation no. f	173	
ν (fitted)	0.44	0.46
Starlike Micelle Model		
R_c (nm)	9.9	
R_m (nm)	16.6	
$\langle R_g^2 \rangle^{1/2}$ (nm)	11.1	

We find a_s to be approximately 1.7 nm, corresponding to 5.5 DMAEMA monomers per statistical segment. From a_s and knowing the copolymer molecular weight, we calculate the number of shell and core segments N_s and N_c. We use these estimates of a_s, N_s, N_c, and f from the SANS data and the exponent $\nu = 0.44$ from the Kratky plots to obtain calculations of R_c, R_g, and R_m from the starlike micelle model. The model also requires a core segment density ρ_c, which we estimate using a_s and the solid-state density of DEAEMA homopolymer. NMR studies have indicated dehydration of the micelle core,[24] so we do not adjust ρ_c to account for possible swelling of the core by water. Values of the parameters used in the starlike micelle model are summarized in Table 2.

DLS and SANS results, as well as calculations from the starlike micelle model are tabulated in Table 3. The measured radii of gyration from the three different fitting methods agree well for the homopolymer, giving an average R_g of 2.6 nm. As expected, the micelle R_g measured using the Zimm approximation is greater than that of the Guinier approximation, giving an average of 14.1 nm for the two approximations. Figure 9 shows Guinier and Zimm plots with the fits used to obtain R_g and $I(0)$ for the homopolymer and micelle samples. The starlike micelle model underestimates the measured micelle R_h and R_g obtained from DLS and SANS.

It is interesting that the underestimation of the model suggests higher degrees of swelling in the micelle corona, whereas the estimate of ν from SANS data suggests sub-θ conditions in the corona. The underestimation of R_g is not as severe as that of R_h, and underestimation of R_h by R_m from the model might be expected as the hydrodynamic drag in the micelle corona causes R_h to appear larger than R_m. Uncertainties in the aggregation number f and the scattering length densities ρ^N used in the model could also contribute to an underestimation of R_h and R_g. In addition, further SANS studies at higher q are planned to obtain more accurate measurements of ν to investigate the apparent sub-θ behavior. Despite the uncertainties, the starlike micelle model qualitatively describes the structure of the DMAEMA/DEAEMA block copolymer micelles. We plan to reexamine, and possibly modify, the existing model to better describe our system.

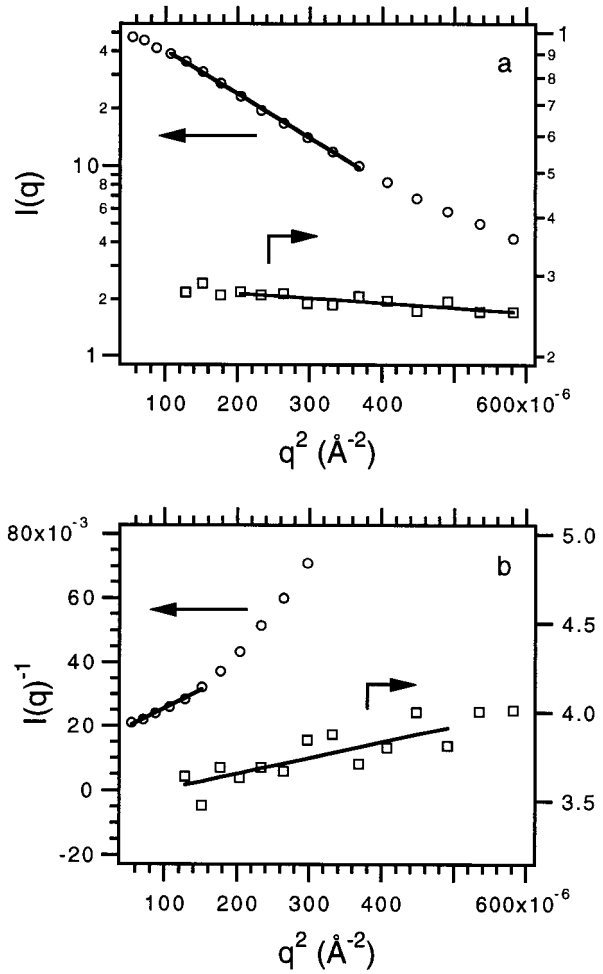

Figure 9. (a) Guinier and (b) Zimm plots of SANS scattering profiles with fits to find R_g and $I(0)$ for (○) DMAEMA/DEAEMA micelles and (□) DMAEMA homopolymer.

Conclusions

We use fluorescence spectroscopy and dynamic light scattering to characterize the structure of DMAEMA/DEAEMA copolymer micelles. Fluorescence results show that the addition of salt allows micellization at higher degrees of protonation because of the screening of the charges. Dynamic light scattering experiments provide unimer and micelle size distributions, and when experiments are performed as a function of acid concentration, we obtain a critical degree of protonation α* and critical pH* consistent with fluorescence results. The DLS results also confirm fluorescence findings that higher salt concentrations allow micellization to occur at higher degrees of protonation. Higher salt concentrations also result in larger radii, resulting from larger micelle aggregation numbers because of the screening of the repulsive charges. Further SAXS and SANS experiments are planned to further investigate this salt dependence. At even higher salt concentrations, the micelles aggregate and come out of solution.[25]

We obtain the micelle radius of gyration and micelle aggregation number from the SANS experiments. Kratky plots of the SANS scattering profiles indicate a sub-θ solvent condition for the chains in the micelle corona; however, further SANS experiments are required to obtain a more accurate picture of the structure in the

micelle corona. Radii calculated using the starlike micelle model tend to underestimate measured values.

We are continuing structural investigations of these copolymer micelles, with the eventual intention of experimentally probing dynamic processes such as equilibrium chain exchange kinetics and the kinetics of micelle breakup or formation.

Acknowledgment. This work was supported primarily by the MRSEC Program of the National Science Foundation under Award Number DMR-9808677. We acknowledge the support of the National Institute of Standards and Technology, U.S. Department of Commerce, in providing the facilities used in the small-angle neutron scattering experiments. We also thank John Pople for his assistance in carrying out the small-angle neutron scattering experiments.

References and Notes

(1) Tuzar, Z.; Kratochvil, P. *Adv. Colloid Interface Sci.* **1976**, *6*, 201.
(2) Halperin, A.; Tirrell, M.; Lodge, T. P. *Adv. Polym. Sci.* **1992**, *100*, 31.
(3) Zhang, L.; Eisenberg, A. *Science* **1995**, *268*, 1728.
(4) Zhang, L.; Yu, K.; Eisenberg, A. *Science* **1996**, *272*, 1777.
(5) Selb, L.; Gallot, Y. Ionic Block Copolymers. In *Developments in Block Copolymers - 2*; Goodman, I., Ed.; Elsevier Applied Science Publishers: New York, 1985; pp 27−96.
(6) Bütün, V.; Billingham, N. C.; Armes, S. P. *Chem. Commun.* **1997**, 671.
(7) Rahman, A.; Brown, C. W. *J. Appl. Polym. Sci.* **1983**, *28*, 1331.
(8) Martin, T. J.; Procházka, K.; Munk, P.; Webber, S. E. *Macromolecules* **1996**, *29*, 6071.
(9) Provencher, S. W.; Hendrix, J.; DeMaeyer, L.; Paulussen, N. *J. Chem. Phys.* **1978**, *69*, 4273.
(10) Provencher, S. W. *Comput. Phys. Commun.* **1982**, *27*, 213.
(11) Provencher, S. W. *Comput. Phys. Commun.* **1982**, *27*, 229.
(12) Vagberg, L. J. M.; Cogan, K. A.; Gast, A. P. *Macromolecules* **1991**, *24*, 1670.
(13) Daoud, M.; Cotton, J. P. *J. Phys. (Paris)* **1982**, *43*, 531.
(14) Cogan, K. A.; Gast, A. P. *Macromolecules* **1991**, *24*, 6512.
(15) Higgins, J. S.; Maconnachie, A. Neutron Scattering from Macromolecules in Solution. In *Polymers in Solution*; Forsman, W. C., Ed.; Plenum Press: New York, 1986; pp 183−238.
(16) Pradny, M.; Seveik, S. *Markomol. Chem.* **1985**, *186*, 111.
(17) Merle, Y. *J. Phys. Chem.* **1987**, *91*, 3092.
(18) Streitwieser, A., Heathcock, C. H., Eds. *Introduction to Organic Chemistry*; Macmillan Publishing Company: New York, 1985.
(19) Kalyanasundaram, K.; Thomas, J. K. *J. Am. Chem. Soc.* **1977**, *99*, 2039.
(20) Wilhelm, M.; Zhao, C.-L.; Wang, Y.; Xu, R.; Winnik, M. A.; Mura, J.-L.; Riess, G.; Croucher, M. D. *Macromolecules* **1991**, *24*, 1033.
(21) Shusharina, N. P.; Nyrkova, I. A.; Khokholov, A. R. *Macromolecules* **1986**, *29*, 3167.
(22) Debye, P. *J. Phys. Colloid Chem.* **1947**, *51*, 18.
(23) Kirste, R. G.; Oberthur, R. C. Synthetic Polymers in Solution. In *Small Angle X-ray Scattering*; Glatter, O.; Kratky, O., Eds.; Academic Press: London, 1982; pp 387−431.
(24) Bütün, V., Ph.D. Thesis, University of Sussex, 1999.
(25) Baines, F. L.; Billingham, N. C.; Armes, S. P. *Macromolecules* **1996**, *29*, 3416.

MA981865O